ORIGINAL

From inside to outside: CT scanning as a tool to link internal knot structure and external branch diameter as a prerequisite for quality assessment

Bruna L. Longo[1,2] · **Franka Brüchert[2]** · **Gero Becker[1]** · **Udo H. Sauter[2]**

Abstract

Branches are as essential for tree growth as knots are detrimental from the wood quality point of view. To bridge the gap between tree growth and the quality toward end-use, this study aims to establish a relationship between internal and external diameters of Douglas-fir whorl branches. The data comprised 102 trees of a wide age range (30–80 years old) from nine study sites in Southwest Germany. External branch measurements were performed in the field following an established protocol. Logs were scanned on a MiCROTEC CT.LOG, and knots were detected by applying an automated algorithm. Obvious detection artefacts by the CT algorithm were excluded to reveal the relationship between inner-outer branch diameters as clear as possible. Results showed a significant mean difference of 13.8 ($\pm$ 10.0) mm between the methods (external diameter being larger), with a model indicating an offset of 9.75 mm and angular shift of 0.53 (RMSE = 7.12 mm; R^2 = 0.57) between the methods. Separate calculations of sound and dead datasets did not reveal a statistically significant difference. By linking the internal knot structure to external branch measurements, the findings of this study constitute a first step toward the incorporation of CT data into growth models, providing a meaningful prediction of the maximum internal knot diameter at an early stage in the wood supply chain.

Introduction

A knot is a wood feature that can greatly affect the value recovery of logs, in particular, Douglas-fir (*Pseudotsuga menziesii* (Mirb.) Franco) logs, as the species is known for its high vigor and growth rate, which often translates into large knots (Hein et al.

✉ Bruna L. Longo
bruna.longo@fobawi.uni-freiburg.de

1 Chair of Forest Utilization, University of Freiburg, Freiburg, Baden-Württemberg, Germany

2 Department of Forest Utilization, Forest Research Institute Baden-Württemberg, Freiburg, Baden-Württemberg, Germany

2008b). The largest branches in Douglas-fir are usually observed in whorls, which is a group of knots that originates at approximately the same height in the tree, with each knot in a different angular position. From the wood production perspective, knots represent a discontinuity in the wood matrix (Grace et al. 2006), causing a reduction in mechanical properties (e.g., strength, stiffness) (Gartner 2005), as well as affecting the visual appearance of the final products (Nyrud et al. 2008; Barbour and Parry 2001; Gartner 2005).

In terms of the wood production chain, foresters are responsible for planting, managing, felling and, sometimes the bucking of trees, ultimately generating roundwood as their final product. By aiming to achieve higher log prices, foresters have, therefore, an interest in acquiring information on the effect of their stand treatment strategies and concepts on the inner quality of logs. To standardize the roundwood quality parameters for trading purposes, log sorting agreements have been established. Regarding knots, these agreements are based on the premise that branches visible from the outside of a log are related to the effect of their inner part (knot) on the sawn timber quality. The European Standard for log sorting (CEN 2008) considers the diameter of the largest knot as a quality criterion, which is measured after debranching at the log surface (surface knot diameter—SKD). The standard differentiates knot diameter thresholds between sound and dead (unsound, loose) knots. For log trades carried out in Germany, the RVR agreement (Anonymous 2015) is commonly used, which has a similar structure to the European standard but applies more restrictive thresholds with regards to allowed dead knot size.

Sawn timber quality is ultimately determined by tree internal characteristics, which cannot be exactly described from outside the log. Sawmillers, in turn, consider these rules when buying the roundwood to convert it to various sawn timber products (e.g., boards, blocks, veneers, etc.). Therefore, predicting internal log quality as early as possible within the forest-wood industry chain is of common interest to both log producers and log consumers, as the aim of both is primarily the same: to efficiently produce and sell good quality wood products. The quality aspect is key here, as it is one of the factors that will influence the product value in different stages of the production chain (Gartner 2005).

Growth models have covered part of the solution for an integration between forest and timber products, by exploring the causal effect of silvicultural treatments on external branch diameter (Väisänen et al. 1989; Hein et al. 2008b; Garber and Maguire 2005; Grace et al. 2015) or directly on saw timber properties (Rais et al. 2014; Högberg et al. 2010), as well as relating branch development to tree measurements (Duchateau et al. 2015) and stand structural data (Mäkinen and Colin 1998). Ultimately, the incorporation of such models into growth simulators (Yue et al. 2013; Dufour-Kowalski et al. 2012) led to its output being linked to product recovery models (Houllier et al. 1995). Tree and stand parameters have also been related to outputs from sawing simulations (Ikonen et al. 2009; Nordmark 2005; Weiskittel et al. 2006), aiming to analyze how silvicultural interventions might affect the final sawn timber quality under several breakdown scenarios. These relationships have mainly covered the effects of forest management on crown aspects, more precisely up to the branch diameter outside the stem (Hein et al. 2008a, 2b, 2009). Other studies focused on knot size issues with regards to processing in sawmills (Fredriksson 2014), relating it to the end product,

either through measurements (Krajnc et al. 2019) or simulated scenarios (Mäkelä et al. 2010). There is, however, a knowledge gap on the relationship between inner and outer branch diameter on the stem/roundwood/log level, due to the different methods required to obtain such measurement information. Such a relationship could pave the way for more robust predictions of internal sawn-timber-oriented parameters from tree or stand measurements.

The acquisition of reliable inner-log measurements has been made possible with advances in non-destructive technologies, of which computed tomography (CT) has been one of the most successful techniques to obtain information on the position and size of internal features of a log (Schad et al. 1996; Longuetaud et al. 2012). Several studies have initially applied the technology to extract internal features, including the knot geometry (Grundberg 1994; Funt and Bryant 1987), which evolved into more advanced algorithms capable of extracting knots automatically (Krähenbühl et al. 2014; Johansson et al. 2013; Longuetaud et al. 2012; Roussel et al. 2014), ultimately leading to sawmill applications, more precisely regarding optimization in terms of log rotation before cutting (Berglund et al. 2013; Fredriksson 2014; Fredriksson et al. 2013; Johansson 2013; Belley et al. 2019), cutting patterns (Ursella et al. 2018) and control of the process (Grundberg 1999).

External branch, respectively, internal knot size as derived from CT scanning is a highly relevant quality indicator both for roundwood and sawn timber. However, CT scanning is primarily a stationary machine in the industry. Despite a study pilot-testing the idea of using the CT technique to decide on log grade for payment (Oja et al. 2010), it is mainly used only after logs have been bought and paid for. CT technology itself does not solve the problem of early prediction of internal features in the forest. In the present approach, CT scanning is used as a methodological tool to obtain internal knot diameter information prior to processing. This way, the internal knot measures are related to external branch size, a measure applied in the forest for log grading. In contrast to recent grading procedures, i.e., EN 1927-3 (CEN 2008) or RVR (Anonymous 2015), which consider only one (i.e., the largest) branch per log for assessment, in this study a higher measurement resolution was chosen, taking into account the largest branch of each whorl of a given log or stem. As a first step toward building a link between external and internal branch characteristics of Douglas-fir trees grown in Southwest Germany, this study aims to establish a quantitative relationship between early measurements of branches from outside the log (on felled trees, with possible application to standing trees in the future) and the inner knots in a log, which are relevant for the quality of processed sawn timber. In addition, this study aimed to analyze such a relationship further by investigating possible differences between sound and dead branches. Then, as a second step, based on such a relationship, it will be possible to predict the internal knot size based on parameters externally measured on whorl or tree level, which will be reported in a subsequent publication.

Material and methods

Sample trees

Data from 102 trees cross-cut to 295 logs, sampled in four earlier scientific projects on Douglas-fir, were used in this study. Within these projects, trees from nine study sites in Southwest Germany, including three age intervals, were sampled. Logs were obtained in 4–5 m sections of the tree merchantable length (up to a minimum log diameter of 7 cm). Detailed information on each project's motivation, goals and methodology can be found in the literature (Abetz 1971; Ehring 2006; Kenk and Hradetzky 1984; Kenk and Thren 1984; Kohnle et al. 2012; Šeho et al. 2013; Šeho and Kohnle 2014). The characteristics of these datasets relevant to this study are summarized in Table 1.

Data structure

This study considered different datasets (Fig. 1). Given that the largest branch per log is crucial for roundwood sorting rules (SKD as base measurement) and that branches usually present larger diameters in whorls than in internodes, this investigation was focused on the maximum branch diameter of the largest branch in a whorl. The CT data available was filtered first to identify only whorl knots, and in a second filtering step, the largest knot per whorl was selected, resulting in the dataset *Raw*. Subsequently, to ensure a reliable dataset for the aforementioned comparison, we visually inspected the CT outputs by comparing the CT images with the

Table 1 Material information on the data used in this study: geographical coordinates (latitude and longitude), number of trees, logs and knots sampled, mean age of the trees (years), mean DBH and tree height (standard deviation)

| Project	Site	Lat (N)	Lon (E)	Tree	Log	Knot	Age (years)	DBH (cm)		Height (m)	
1	Schluchsee	47° 84′	8° 11′	10	30	160	53	48.8	3.5	30.0	1.7
1	Schwetzingen	49° 28′	8° 58′	10	21	97	53	45.3	2.5	33.0	1.2
1	Sindelfingen	48° 70′	9° 06′	10	26	135	53	47.8	4.0	32.0	1.7
2	Ehingen	48° 17′	9° 37′	5	19	32	41	44.6	11.1	30.3	3.2
2	Löwenstein	49° 04′	9° 25′	5	15	28	42	46.0	9.3	32.2	2.1
2	Kandern	47° 42′	7° 42′	5	15	25	44	46.9	9.5	33.0	2.5
3	Kandern	47° 42′	7° 42′	30	96	340	49	46.7	10.8	34.2	3.0
4	Höllental	47° 56′	8° 0′	8	41	216	78	69.4	4.6	47.2	1.8
4	Odenwald	49° 33′	9° 16′	19	32	144	32	32.8	7.1	26.6	2.1
Total				102	295	1177					
Minimum								32.8		26.6	
Mean								47.6		33.2	
Maximum								69.4		47.2	
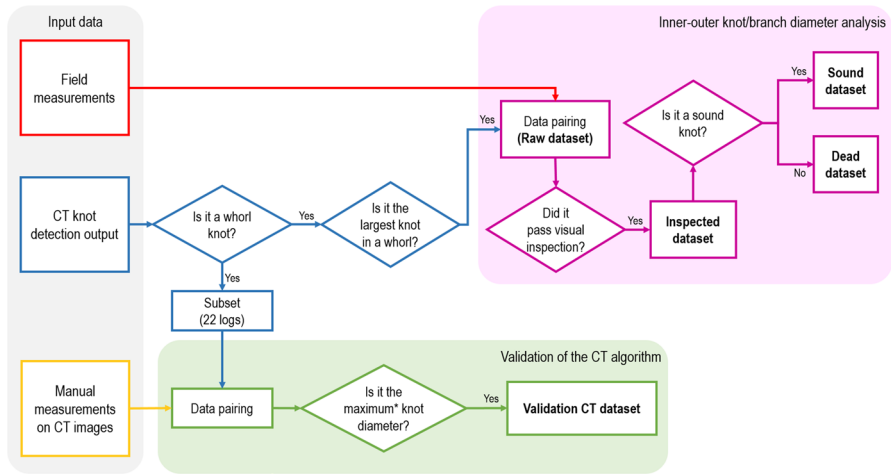
Fig. 1 Description of the data structure. Colours represent the origin of the data being considered (red, blue and yellow depict, respectively, the field measurements, CT automated output and manual measurements on CT images; purple and green show, respectively, steps that considered the first two and the latter two data inputs. Bold terms indicate the name of the generated dataset. *Maximum knot diameter here refers to the largest diameter found in the radial direction, between stem pith and bark, for each largest knot in a whorl (colour figure online)

automated CT detected knot data. Obvious cases of misdetection between detected knots and the underlying CT image were eliminated, resulting in a subset of the previous dataset: *Inspected*. To evaluate possible differences in this relation due to knot status (sound and dead knots), the Inspected dataset was split according to this factor, resulting in the datasets *Sound* and *Dead*.

Knot detection as mentioned in the previous procedure was completely automated. Therefore, it was validated against manual measurements on CT images, to provide criteria of precision and accuracy. The aim here was to verify how the knot detection algorithm performed in providing the maximum knot diameter in a given whorl. For this validation analysis, we selected only whorl knots from the CT data and compared them with the respective knot data from manual measurements on CT images, generating the *Validation CT* dataset (Table 2; Fig. 1).

Diameter of the largest branch per whorl (field data)

The technical preparation of the trees composing the material of this study followed an internal protocol, based on which they were felled and bucked into 3–5-m-length logs. The debranching of these trees was delayed until all measurements were finished. Groups of at least three branches that occurred at the same height in the stem were identified as whorls. Moreover, the distance between whorls and the counting of annual rings in both crosscut faces of each log were considered as a verification of the whorls.

Table 2 Material information on the subset of data used for the validation of the CT algorithm, including: geographical coordinates (latitude and longitude), number of trees, logs and knots sampled, mean age of the trees (years), mean DBH and tree height (standard deviation)

Project	Site	Lat (N)	Lon (E)	Tree	Log	Knot	Age (years)	DBH (cm)	Height (m)
1	Schluchsee	47° 84′	8° 11′	2	2	59	53	44.1 $^{0.4}$	27.9 $^{1.1}$
1	Schwetzingen	49° 28′	8° 58′	2	2	54	53	47.8 $^{3.1}$	32.5 $^{0.9}$
1	Sindelfingen	48° 70′	9° 06′	2	2	78	53	50.8 $^{4.6}$	32.5 $^{1.3}$
2	Löwenstein	49° 04′	9° 25′	1	4	292	42	51.8 $^{-}$	34.6 $^{-}$
4	Höllental	47° 56′	8° 0′4	6	6	149	78	69.8 $^{5.2}$	47.6 $^{1.4}$
4	Odenwald	49° 33′	9° 16′	6	6	249	32	33.2 $^{4.9}$	27.0 $^{1.7}$
Total				19	22	881			
Minimum							32.0	33.2	27.0
Mean							53.7	50.2	35.1
Maximum							78.0	69.8	47.6

The diameter of the largest branch per whorl was determined as the mean of two crossed diameter measurements perpendicular to the branch axis, taken with a caliper (± 0.5 mm). To avoid overestimation of this variable, the exact measurement position (axial distance from the stem surface) varied, since we tried to minimize the effect of the branch collar (Shigo 1985). The whorl longitudinal position along the stem was recorded as the distance to the ground of the lowest branch in this whorl, according to a specific protocol (Brüchert et al. 2017). Whorls that only consisted of (overgrown) branch scars, or in case the largest branch was broken, were counted but not measured.

Diameter of the largest knot per whorl (CT data)

Logs were transported to the Forest Research Institute of Baden-Württemberg (FVA), where they were scanned using the MiCROTEC CT.LOG scanner (Giudice-andrea et al. 2011). The scanning process generated sinograms that were converted into stacked grey-level images. Each image presented a cross-cut view with a pixel size of 1.107×1.107 mm representing 5 mm of the log length. By positioning a group of such consecutive images in a row, a 3D virtual log can be generated.

The internal knot structure was derived by processing these stacked images. This step was automatically carried out using the following established algorithms for the detection of: (1) the stem pith (Boukadida et al. 2012); (2) borders, such as heartwood-sapwood, wood-bark and outer border (Longuetaud et al. 2007; Baumgartner et al. 2010); and (3) knots (Johansson et al. 2013). The algorithm configurations were set as defined by Longo et al. (2019a) in a study in which the authors presented knot detection filter configurations adjusted for Douglas-fir, as well as accuracy results.

The knot detection algorithm fits ellipses (Fig. 2B) to roughly round-shaped areas with distinctly higher values (i.e., lighter shades), which correspond to knots
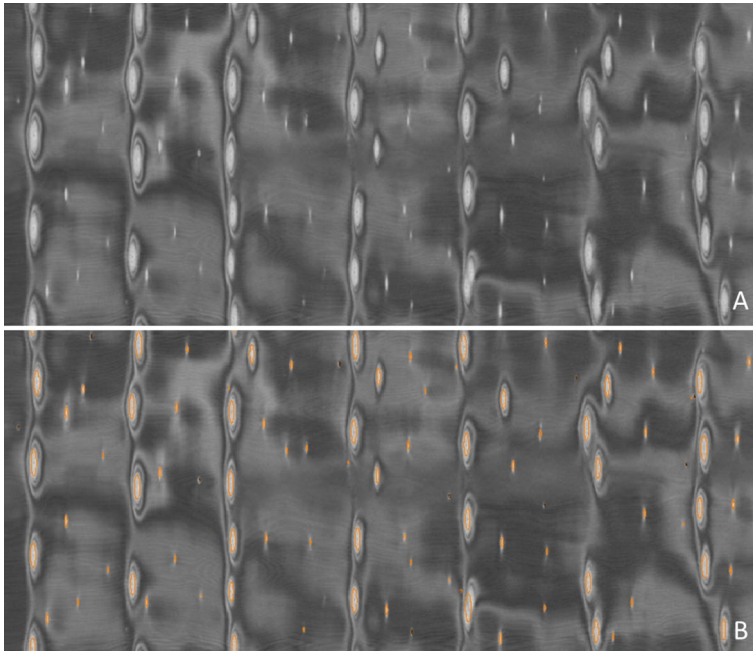
Fig. 2 Unprocessed CT image of a log (**A**) and the knot detection result based on ellipse fitting (**B**). The image presents the internal surface of the log at a radial distance of 60 mm from the stem pith. Longitudinal and angular positions are represented by horizontal and vertical axes, respectively. Regarding colors, the reader is referred to the digital version of this article

(Fig. 2A). The ellipse fitting process is performed radially in relation to the stem pith, in ten positions along the pith-bark gradient. Due to better image contrast between knots and the surrounding wood, the algorithm was designed to locate at least five positions within the heartwood area. Ultimately, based on ten ellipses detected along the stem radius, the algorithm fits a knot diameter model (Grönlund et al. 1995) with a unique parameterization for each knot (Eq. 1).

$$\phi(r) = A + B\sqrt[4]{r} \tag{1}$$

where $\varphi(r)$ is the arc (in rad) corresponding to the knot aperture at a given r radial position from the stem pith (in mm); A and B are parameters generated uniquely for each knot based on the algorithm's knot detection.

This model generates the arc corresponding to the knot diameter aperture at a given radial position. To acquire the linear knot diameter, i.e., the smaller distance between two points (both extremities of the knot aperture), a transformation of the variable was necessary (Eq. 2).

$$D(r) = \left| \tan\phi_{(r)} * 2r \right| \tag{2}$$

where $D(r)$ is the linear knot diameter at the r radial position (in mm) from the stem pith (in mm).

The maximum diameter of sound knots extracted by the algorithm is at the outermost radial position within the stem, i.e., the position right under the bark. In this situation, the corresponding branches are still functional; thus, their size is expected to grow further. Dead knots, in contrast, show the peak of their diameter development inside the stem: their maximum diameter is considered within the algorithm as the point after which the knot size is expected either to directly decrease or to remain constant and then to decrease. In cases where dead knot diameters remain constant, the innermost maximum value is considered.

Validation of the CT knot detection algorithm

Although Longo et al. (2019a) have carried out a validation of the knot detection algorithm on Douglas-fir knots in general, a further validation was performed in this study focusing on the accuracy of the algorithm in detecting the maximum knot diameter of whorl knots (large or small). The material for this validation consisted of 22 logs selected randomly out of 295 logs available for this study. In the CT images of these logs, all whorls were visually identified, and the vertical maximum diameter of each knot belonging to a given whorl was manually measured. In total, the maximum diameter of 881 manually measured knots was paired with the CT automated output (*Validation CT* dataset), identified according to their longitudinal and azimuthal positions.

Knot-branch measurement pairing

The pairing of internal and external measurements was performed in two steps: (1) whorls were matched based on their longitudinal position (± 10 cm); (2) the largest knot detected per whorl was assigned to the largest branch measurement. Due to overestimation and underestimation from the knot detection algorithm (Longo et al. 2019a), the largest knot detected by the algorithm might not always be the largest knot in reality. Therefore, all whorls were verified in the CT images after the automatic knot detection to ensure that the CT data contained the largest knot (pairing step in Fig. 1). The verification was mainly visual, but in cases where two or more knots presented visually similar sizes, a measurement of each doubtful knot was performed (on the CT image) at its outermost position under bark. The largest knot was then manually assigned to that particular whorl (if it was not already the case). In cases where no matching between CT and field datasets was possible (due to, e.g., the largest knot being undetected or not measured in the field, height position differences higher than 10 cm), the whorl in question was ignored in the analysis. These three steps generated the first paired dataset (*Raw* dataset, Fig. 1).

Visual inspection of CT images

In a further step, the aim was to check for the presence of technical artefacts. Since the field data cannot be re-measured, a visual inspection was conducted only on CT data, aiming to check for detection inconsistencies (incomplete detection, and knot sizes and shapes beyond plausibility). As a result of this inspection, errors were identified as a consequence of natural occurrences (crack through the stem or through the knot, group of knots, subsequent knots, steep knots, extrapolated wood-bark border and large occluded knots). Implausible cases were identified when the detection was clearly not representing the respective knot (shape, size or orientation) at the peak of its internal development (i.e., maximum diameter position). The overall knot detection could have been very good, but if the detected knot clearly did not reflect the actual knot at the maximum diameter point, this knot was also removed during the inspection. Thus, only knots that were not affected by the aforementioned inconsistencies remained in the analysis, referred to as *Inspected* dataset, Fig. 1.

Data analysis

In the validation of the CT algorithm, a detection rate and the number of falsely detected instances (non-existent but detected as "knots") were derived by comparing manually measured knots with knots detected by the algorithm (*Validation CT*). The detection rate was calculated by dividing the number of correctly detected knots by the total number of knots. In addition, the number of falsely detected knots was recorded. The comparison between the measurements from both methods was described by the mean absolute error (MAE), standard deviation of the errors (SDE), the Pearson correlation coefficient (ρ) and the 95% limits of agreement (LAE, calculated as $MAE \pm 1.96*SDE$) according to Bland and Altman (2003). The latter returns a probabilistic knot diameter error range. In addition, the concordance correlation coefficient (ρ_c) was calculated (Lin 1989, 2000), which provides a measure of how precise the data are compared to a perfect match scenario between the two methods. Lin's concordance correlation coefficient varies from -1 to 1 and quantifies the distance from the reference line ($x = y$). According to the author, such a coefficient can be further explored by analyzing the scale (v) and location (u) shift parameters, which indicate the weight of each type of shift from the reference line, as they diverge from 1 and 0, respectively. In addition, the analysis of the C_b parameter reveals how different the best-fit line is in comparison with the reference $x = y$ line as it deviates from 1. The C_b parameter is a measure of accuracy and is calculated as a correction factor between ρ_c and ρ, i.e., the quotient between ρ_c and ρ (Lin 1989, 2000).

In the inner-outer knot/branch diameter analysis, a summary of the descriptive statistics was produced for each dataset (*Raw*, *Inspected*, *Sound* and *Dead*). To examine whether the knot diameter difference between field and CT dataset was statistically significant ($D_{\text{Field}} - D_{\text{CT}}$), a paired *t* test with 0.05 of significance

threshold was calculated for each of the four datasets. In addition, to establish how these two variables relate to each other a linear model was fitted (Eq. 3).

$$D_{CT} = b_0 + b_1 D_{Field} + \varepsilon_i \text{ with } \varepsilon_i \sim N\left(0, \sigma^2\right) \tag{3}$$

where D_{CT} is the internal knot diameter automatically detected by the CT algorithm; D_{Field} is the external branch diameter measured in the field; estimates b_0 and b_1 are the intercept and slope of the model, respectively; and ε_i represents the information unexplained by the previous components, following a normal distribution with mean 0 and variance σ^2.

For the comparison of the parametric mean differences between sound and dead knot groups, the Welch's two sample t test was applied. According to Delacre et al. (2017), the Welch t test should be preferred (over, e.g., the Student's t test) independently of the samples' variances assumption, for cases where the samples being tested follow a normal distribution but have a different number of observations (unpaired samples).

Data management and analyzes throughout this study were performed in R (R Core Team 2016), using the following additional packages: epiR (Stevenson et al. 2018), dplyr (Wickham et al. 2019), broom (Robinson and Hayes 2019), ggplot2 (Wickham 2016) and gridExtra (Auguie 2017).

Results and discussion

Validation of the CT algorithm

The CT automated algorithm detected 881 whorl knots, from a total of 1016 whorl knots that were identified in the CT images (*Validation CT* dataset). In addition, 33 falsely detected knots were observed in whorl areas. In this dataset, the manual measurement (on CT images) method had a mean knot diameter of 10.3 mm (standard deviation = 5.91 mm), while the automated CT method found a mean value of 10.8 mm (standard deviation = 5.6 mm). The mean absolute error between the two diameter measurements was 0.48 mm (standard deviation of 2.70 mm). The results presented good precision ($\rho = 0.89$), with slight shift from the reference line, as shown by both scale ($v = 0.94$) and location ($u = 0.08$) parameters. These parameters show that the best-fit line is unbiased and not shifted in comparison with the $x = y$ reference line. This behavior can be seen in Fig. 3A, which illustrates how measurements from both methods compare. In addition, ρ_c (0.89; with confidence interval of 0.87–0.90) and C_b (0.99) corroborate the performance observed, as they approach 1. The limits of agreement were -5.77 and 4.81 mm, as presented in Fig. 3B. This plot was recommended by Altman and Bland (1983) as a tool to avoid letting the range of measurements influence the appearance of graphic agreement, since it shows the difference between the methods against the mean between them.

The knot detection algorithm identified 86.7% of all whorl knots on CT images on the *Validation CT* dataset. In a previous study (Longo et al. 2019a), a validation of the same knot detection algorithm was performed on 15 Douglas-fir logs,
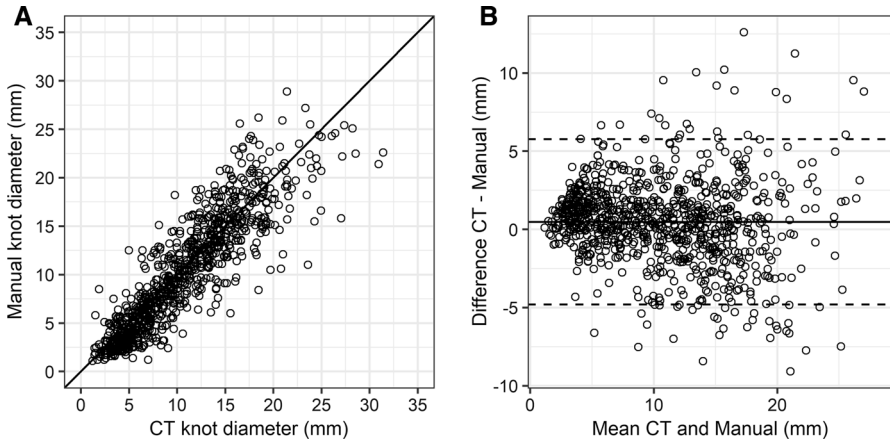
Fig. 3 Validation of the CT knot diameter against manual measurements on CT images, in which (**A**) presents the alternative versus the reference method, and (**B**) presents the mean versus the difference between the methods (Bland–Altman plot). The full line represents the reference line ($x = y$) in (**A**), and the mean difference between the variables in (**B**). Dashed lines show the 95% limits of agreement

in which several measurements along the radial gradient of whorl knots and inter-nodes were accounted for. That study observed a higher detection rate of 93.9%. With regards to the algorithm's accuracy, the aforementioned study showed mean diameters of 22.4 and 23.7 mm, respectively, for manual and CT methods, resulting in a MAE of 1.34 mm (manual—CT), SDE of 7.72 mm and a ρ_c of 0.82. The differences observed between the results of the current study and the ones presented in Longo et al. (2019a) are mainly due to the aim of each study and the data considered in each investigation. The aforementioned study used old Douglas-fir trees (approx. age of 78 years), covering knots in general, accounting for as much small knots as larger ones, in whorls and internodal ones, and with measurements taken along the knot length, providing an overview of the overall accuracy of the algorithm. In turn, the current study utilizes a broader range of tree age, focuses on whorl areas, and considers only the maximum diameter of such knots.

Comparison between external branch measurements and CT knot detection results

The analysis of the *Raw* dataset comprised 1198 matched pairs of internal knot and external branch diameter (Table 3). The descriptive statistics of the dataset revealed a statistically significant (p < 0.05, Table 4) mean difference of 23.7 mm (± 13.9 mm). The linear model showed a low capability to explain the variability present in this dataset ($R^2 = 0.23$). Figure 4A indicated possible agreement issues, in which points showed suspicious differences between the two diameters. A slight tendency could be seen in Fig. 4C, between the residuals to the reference line and the external branch diameter measurements. The *Inspected* dataset accounted for 288 knot pairs (from 84 trees and 156 logs) and was used to analyze the relation

Table 3 Descriptive statistics of the different datasets regarding branch size (in mm)

Dataset	Measurement	N	Min	Max	Mean	SD
Raw	Field	1198	17.0	106.0	49.4	14.4
	CT	1198	1.90	73.0	25.8	12.5
Inspected	Field	288	19.7	103.0	50.7	15.3
	CT	288	13.4	73.0	36.9	10.8
Sound	Field	102	26.0	103.0	54.0	16.4
	CT	102	16.7	73.0	39.8	11.9
Dead	Field	186	19.7	94.0	48.5	14.4
	CT	186	13.4	69.8	35.3	9.90
Validation	Manual	881	1.10	28.9	10.3	5.91
	CT	881	1.20	31.4	10.8	5.59

N: sample size; SD: standard deviation

Table 4 Descriptive and paired t test statistics of the differences (=external—internal) between branch diameters for the different datasets

Dataset	Min	Mean	Max	SD	t-statistic	df	p-value	CI
Raw	− 18.4	23.7	94.8	13.9	59.0	1197	2.20E−16	[22.9; 24.4]
Inspected	− 10.5	13.8	54.5	10.0	23.3	287	2.20E−16	[12.6; 15.0]
Sound	− 5.9	14.2	37.6	10.1	14.2	101	2.20E−16	[12.2; 16.2]
Dead	− 10.5	13.6	54.5	10.0	18.4	185	2.20E−16	[12.1; 15.0]

SD: standard deviation; df: degrees of freedom; CI: 95% confidence interval. All values are in mm
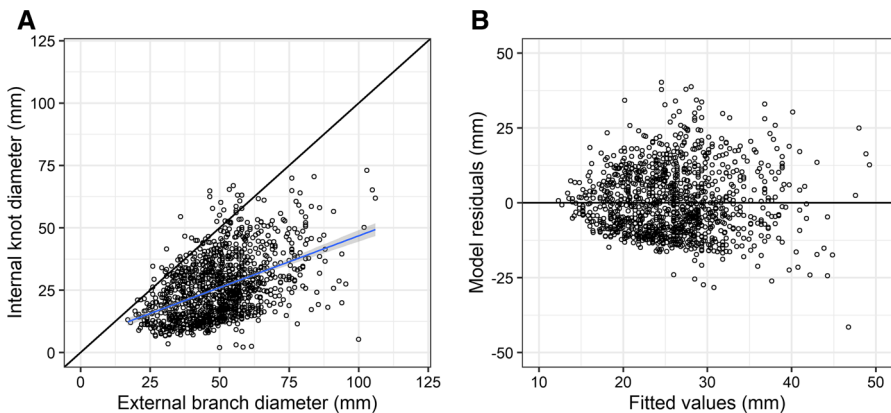

Fig. 4 Results of model fitting on the relation between CT and field measurements before visual inspection on CT images. Sample size: 1198 knots. Black lines represent reference lines (in **A** is the $x = y$ relation, and in **B** is the zero deviation of the residuals). The blue line depicts the linear model fitted to the data and the shading area surrounding it represents the 95% confidence interval of the mean model. Regarding colors, the reader is referred to the digital version of this article (colour figure online)
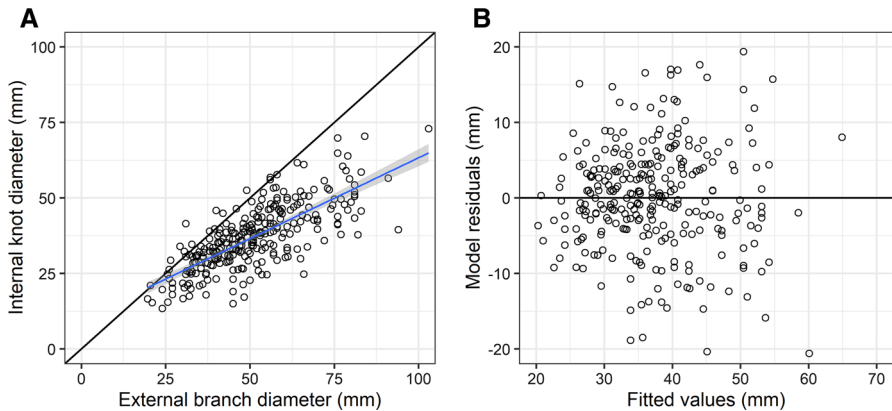
Fig. 5 Results of model fitting on the relation between CT and field measurements after visual inspection on CT images. Sample size: 288 knots. Black lines represent reference lines (in **A** is the $x=y$ relation, and in **B** is the zero deviation of the residuals). The blue line depicts the linear model fitted to the data and the shading area surrounding it represents the 95% confidence interval of the mean model. Regarding colors, the reader is referred to the digital version of this article (colour figure online)

Table 5 Results of the model fitting for the different datasets considered

Dataset	N	b_0	b_1	RMSE	R^2
Raw	1198	5.26 [(1.14)]	0.41 [(0.02)]	11.04	0.23
Inspected	0288	9.75 [(1.46)]	0.53 [(0.03)]	7.12	0.57
Sound	0102	8.72 [(2.54)]	0.58 [(0.04)]	7.39	0.62
Dead	0186	11.27 [(1.79)]	0.49 [(0.04)]	6.89	0.51

N: sample size; b_0 and b_1: intercept and slope of the model, respectively (in mm); RMSE: root mean square error (in mm); R^2: coefficient of determination

between knot and branch measurements (Fig. 5A). It showed a statistically significant difference between internal and external diameters according to the paired t test ($p < 0.05$), with no clear pattern in the residuals (Fig. 5B). Regarding the model depicted in Fig. 5A, the intercept value indicates that external measurements are 9.75 mm larger than the CT internal diameter (Table 5). The model's angular coefficient (b1 = 0.53) indicates that the relationship has a positive trend, but also that the difference between external branch diameter and the respective predicted internal diameter increases at a lower rate as branches increase in size.

The present results showed that the relation between the external branch diameter measurements performed in the field and the maximum internal knot diameter acquired by means of CT technology is linear. In Fig. 5A, the model line intercepts the reference ($x=y$) line at a branch diameter of 20.74 mm, indicating that below such a point, the model would estimate negative values of internal knot diameter. This was likely due to the fact that this range of data (small knots; below 20 mm of diameter) was not sampled in this study, as only the largest branch per whorl was considered. Pyörälä et al. (2018) compared external and internal knot diameter

measurements of Scots pine (*Pinus sylvestris* L.) using Terrestrial Laser Scanning (TLS) of standing trees and X-ray scanning of the corresponding logs, respectively. The authors found a significant mean difference of 6.5 mm for maximum knot diameter between the methods (TLS—X-ray). Such a difference was attributed to the internal knot diameter acquisition method (single-directional X-ray digital radiograph scanner) and to the estimation of the maximum knot diameter per whorl, which was based on "the length of the whorl along the stems longitudinal axis in the X-ray images, which is sensitive to noise and overlapping knots". Furthermore, the authors mentioned that the external measurements are affected by wind, which likely causes an increasing registration error on the TLS point cloud toward the treetops. In the present study, the observed differences between the measurement results might be explained by the distinct measurement positions along the axis of the branch and the branch bark thickness present in the external measurement. Differences are also found in the knot definition, i.e., the outlining rule that defines the boundaries of a knot, when examining knots internally and externally applying distinct methods. External branch measurements contribute to deviations in this inner-outer knot/branch diameter relation due to the presence of bark, characterizing the field measurement as a diameter with double bark thickness; branch collar (Shigo 1985), measurement errors, and considering that external branch diameter is inversely related to the position in branch length (Fernández and Norero 2006), to inaccuracies of measurement positions. In turn, internal knot measurements in the log periphery using CT techniques present poor knot-stem wood matrix contrast in the sapwood region (Funt and Bryant 1987; Longuetaud et al. 2012; Wei et al. 2009; Breinig et al. 2012; Fredriksson et al. 2017; Johansson et al. 2013). As a consequence, the increment in knot diameter in this region might be overlooked, due to smooth boundaries (especially in sound knot cases). Moreover, we observed that the CT method is influenced by technical aspects (image resolution, quality and contrast in different areas), as well as the biological configuration of the material (knot distribution and positioning).

Furthermore, the visual identification of whorls in the field or when analyzing CT images can pose a challenge when analyzing paired data from different methods. In the field, the number of whorls can be roughly verified by comparing the annual rings at the top and bottom positions of the stem section and consequently comparing the difference between those to the number of whorls in that section. On the other hand, visually identifying whorls in large CT datasets is very onerous, time consuming and susceptible to visual errors. However, the density distribution along the stem height provided by analyzing CT images might reveal whorl footprints (Longo et al. 2019b; Longuetaud et al. 2005), which could be used for automated whorl detection, reducing errors related to whorl interpretation.

As the extraction of sound and dead knots' diameter in the CT detection follows different approaches, the *Inspected* dataset was split in two subgroups representing the different knot status. Figure 6 presents the visualization of the results for these two knot groups. The linear tendency was maintained, with field measurements presenting mean values of 14.2 ($\pm$ 10.1) and 13.6 ($\pm$ 10.0) mm higher than the CT knot diameter for sound and dead knots, respectively. Although the goodness of fit for sound knots is higher than for dead knots, the spread of data in both groups is very
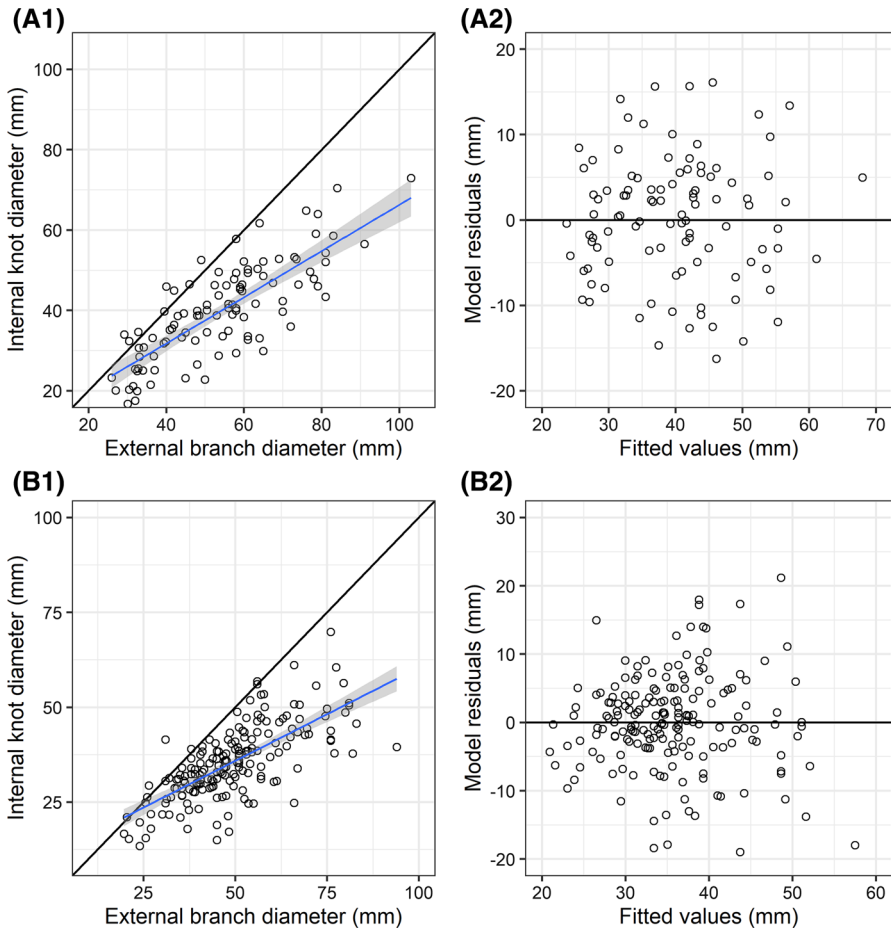
(A1)

(A2)

(B1)

(B2)

Fig. 6 Results of model fitting on the relation between CT and field measurements after visual inspection on CT images, detailing groups of sound (**A**) and dead (**B**) knots. Sample size: 102 (sound) and 186 (dead) knots. Black lines represent reference lines (in 1 is the $x=y$ relation, in 2 is the zero deviation of the residuals). The blue line depicts the linear model fitted to the data, and the shaded area surrounding it represents the 95% confidence interval of the mean model. Regarding colors, the reader is referred to the digital version of this article (colour figure online)

similar. According to the Welch test, the disparity of the mean difference between the groups is not statistically significant ($t=0.51$; $df=203.6$; p-value$=0.61$). In addition, in Fig. 5A, the point in which the model line intercepts the reference line should split sound and dead knot groups. However, as also observed in Table 4 and Fig. 6, this is not the case. Negative minimum values in Table 4, as well as the region lower than the intercept between the lines in Figs. 5A, 6A1, A2 mean that we observed larger D_{CT} than its respective external counterpart D_{Field} at times. It was expected that inner-outer branch diameter differences for dead knots would gravitate around zero or even negative values ($D_{Field} - D_{CT}$). This was based on the knot

status definition within the applied CT algorithm (Johansson et al. 2013), in which a knot is considered dead when it has reached its development peak within the stem, i.e., the maximum knot diameter found somewhere between pith and bark. Theoretically, after this point the knot stops growing, and its diameter might be constant for some time or directly decrease. However, this was not the main observed behavior in the present study. There were a few dead knots that would confirm this pattern, but the majority showed differences similar to a sound knot instance, i.e., further growth. This behavior could be due to thicker branch bark in dead branches, which was not noticed in the field. The most probable cause is a misclassification from the algorithm, identifying sound knots as dead ones, as found in a previous study (Longo et al. 2019a). Only considering the maximum knot diameter might not be sufficient to accurately identify the sound-dead border of a knot. In fact, evidence was found in a study on Douglas-fir branch radial growth that after the maximum diameter has been reached, the knot might still be sound for an average of 8 (±4.7) years (Kershaw et al. 1990), presenting no differences in diameter. Therefore, we understand that there is an uncertainty regarding the sound-dead boundary of a knot when applying CT images to identify the status of a knot, since deviations in knot detection might lead to a false maximum diameter point. In this context, further studies on branch mortality and its identification on material grown and adapted in the region might lead to improvements of the sound-dead border detection within the algorithm.

Conclusion

This was, to the authors` knowledge, the first study on Douglas-fir logs to relate external whorl branch diameters from field measurements and internal knot diameters using a CT automated knot detection algorithm. A linear relation was evidenced after CT detection inconsistencies were excluded. No difference in the inner-outer branch diameter relation between sound and dead knot data was found to be significant. The findings of this study must be considered along with the limitations of the methods. Probable influencing factors identified were related to the automated CT detection (whorl identification, steep knots, sapwood effect, smooth knot boundaries in sound knots) and to the field data acquisition (the presence of bark, branch collar and measurement errors). Developments in the knot detection process (pith, borders and knot detection algorithms) might improve the accuracy of measurements acquired from CT data.

As the inner maximum knot diameter relates to the knot morphology more precisely than the external branch diameter, this information is also realistically closer to the branch diameters in the final timber products (Duchateau et al. 2013). Future work should concentrate on predicting the internal knot diameter based on external measurements obtained in the forest, which could be potentially either measured at the log surface (SKD) or remotely on standing trees (e.g., with photo-optical or laser sensing technology) in the course of inventory measurements in the field. As we understand the relationships between different stages of this process (remote sensing, felled tree measurements, internal measurements), we will likely unlock

possibilities, such as: enabling a more reliable roundwood quality assessment (oriented toward the end-user) via model predictions and providing more accurate internal knot metrics when refining existing forest growth models to include a prediction of wood quality at an early point in the wood supply chain.

Authors contributions Bruna L. Longo and Franka Brüchert contributed to the study conception and design. Material preparation, data collection and analysis were performed by Bruna L. Longo. Franka Brüchert, Gero Becker and Udo H. Sauter supervised the work. The first draft of the manuscript was written by Bruna L. Longo, and all authors commented on previous versions of the manuscript. All authors read and approved the final manuscript.

Availability of data and materials The datasets analyzed in this study are available from the corresponding author on reasonable request.

Declarations

Conflict of interest All authors declare that they have no conflict of interest.

References

Abetz P (1971) Douglasien-Standraumversuche. Afz/der Wald 26:448–449

Altman DG, Bland JM (1983) Measurement in medicine. The analysis of method comparison studies. J R Stat Soc Ser D (Stat) 32(3): 307–317.

Anonymous (2015) *Rahmenvereinbarung für den Rohholzhandel in Deutschland (RVR) des Deutschen Forstwirtschaftsrates e.V. und des Deutschen Holzwirtschaftsrates e.V.* [Framework Agreement for the Raw Timber Trade in Germany (RVR) of the German Forestry Council and the German Timber Industry Council] 2nd updated edition

Auguie B (2017) *gridExtra: Miscellaneous Functions for "Grid" Graphics.* R package version 2.3. https://CRAN.Rproject.org/package=gridExtra. Accessed 15 September 2020

Barbour RJ, Parry DL (2001),Log and lumber grades as indicators of wood quality in 20- to 100-year old Douglas-fir trees from thinned and unthinned stands, General Technical Report PNW-GTR-510. Portland, Oregon

Baumgartner R, Brüchert F, Sauter UH (2010) Knots in CT scans of pine logs. In: The future of quality control for wood and wood products, the final conference of COST Action E53, Edinburgh, United Kingdom, 4–7 May 2010. Dan Ridley-Ellis and John Moore (eds)

Belley D, Duchesne I, Vallerand S, Barrette J, Beaudoin M (2019) Computed tomography (CT) scanning of internal log attributes prior to sawing increases lumber value in white spruce (*Picea glauca*) and jack pine (*Pinus banksiana*). Can J for Res 49(12):1516–1524

Berglund A, Broman O, Grönlund A, Fredriksson M (2013) Improved log rotation using information from a computed tomography scanner. Comput Electron Agric 90:152–158

Bland JM, Altman DG (2003) Applying the right statistics: analyses of measurement studies. Ultrasound Obstet Gynecol 22:85–93

Boukadida H, Longuetaud F, Colin F, Freyburger C, Constant T, Leban JM, Mothe F (2012) PithExtract. a robust algorithm for pith detection in computer tomography images of wood—application to 125 logs from 17 tree species. Comput Electron Agric 85:90–98

Breinig L, Brüchert F, Baumgartner R, Sauter UH (2012) Measurement of knot width in CT images of Norway spruce (Picea abies [L.] Karst.)—evaluating the accuracy of an image analysis method. Comput Electron Agric 85:149–156

Brüchert F, Baumgartner R, Montoya DH, Sauter UH (2017) FastForests: impacts of faster growing forests on raw material properties with consideration of the potential effects of a changing climate on species choice, available at: https://www.fnr.de/index.php?id=11150&fkz=22005714. Accessed 28 July 2020

CEN (2008) CEN 1927-3. 2008-6: Qualitative classification of softwood round timber: Part 3: Larches and Douglas fir, Deutsches Institut für Normung, Berlin

Delacre M, Lakens D, Leys C (2017) Why psychologists should by default use Welch's t-test instead of Student's *t*-test. Int Rev Soc Psychol 30(1):92

Duchateau E, Longuetaud F, Mothe F, Ung C, Auty D, Achim A (2013) Modelling knot morphology as a function of external tree and branch attributes. Can J For Res 43(2):266–277

Duchateau E, Auty D, Mothe F, Longuetaud F, Ung CH, Achim A (2015) Models of knot and stem development in black spruce trees indicate a shift in allocation priority to branches when growth is limited. PeerJ 3:e873

Dufour-Kowalski S, Courbaud B, Dreyfus P, Meredieu C, Coligny F (2012) Capsis. An open software framework and community for forest growth modelling. Ann For Sci 69(2):221–233

Ehring A (2006) "Ergebnisse aus dem Douglasien-Standraumversuch" (Results from the Douglas fir stand trial) (in German). FVA-Einblick 10(3):15–17

Fernández MP, Norero A (2006) Relation between length and diameter of *Pinus radiata* branches. Scand J For Res 21(2):124–129

Fredriksson M (2014) Log sawing position optimization using computed tomography scanning. Wood Mater Sci Eng 9(2):110–119

Fredriksson M, Johansson E, Berglund A (2013) Rotating *Pinus sylvestris* sawlogs by projecting knots from X-ray computed tomography images onto a plane. BioResources 9(1):816–827

Fredriksson M, Cool J, Duchesne I, Belley D (2017) Knot detection in computed tomography images of partially dried jack pine (*Pinus banksiana*) and white spruce (*Picea glauca*) logs from a Nelder type plantation. Can J For Res 47(7):910–915

Funt BV, Bryant EC (1987) Detection of internal log defects by automatic interpretation of computer tomography images. For Prod J 37(1):56–62

Garber SM, Maguire DA (2005) Vertical trends in maximum branch diameter in two mixed-species spacing trials in the central Oregon Cascades. Can J For Res 35(2):295–307

Gartner BL (2005) Assessing wood characteristics and wood quality in intensively managed plantations. J Forest 103(2):75–77

Giudiceandrea F, Ursella E, Vicario E (2011) A high speed CT-scanner for the sawmill industry. In: 4–16 September 2011, Sopron, Hungary, University of West Hungary

Grace JC, Pont D, Sherman L, Woo G, Aitchison D (2006) Variability in stem wood properties due to branches. NZ J Forest Sci 36(2/3):313–324

Grace JC, Brownlie RK, Kennedy SG (2015) The influence of initial and post-thinning stand density on Douglas-fir branch diameter at two sites in New Zealand. NZ J Forest Sci 45(1):14

Grönlund A, Björklund L, Grundberg S, Berggren G (1995) Manual för Furustambank. [Manual of the Pine Stem Bank.], Luleå

Grundberg S (1994) Scanning for internal defects in logs. Licentiate thesis, Luleå University of Technology, Skellefteå, Sweden. ISSN 0280-8242

Grundberg S (1999) An X-ray LogScanner—a tool for control of the sawmill process. Doctoral thesis, Luleå University of Technology, Skellefteå, Sweden. ISSN 1402-1544

Hein S, Weiskittel AR, Kohnle U (2008a) Branch characteristics of widely spaced Douglas-fir in southwestern Germany. Comparisons of modelling approaches and geographic regions. For Ecol Manage 256(5):1064–1079

Hein S, Weiskittel AR, Kohnle U (2008b) Effect of wide spacing on tree growth, branch and sapwood properties of young Douglas-fir [*Pseudotsuga menziesii* (Mirb.) Franco] in south-western Germany. Eur J Forest Res 127(6):481–493

Hein S, Weiskittel AR, Kohnle U (2009) Models on branch characteristics of wide-spaced Douglas-fir. In: Dykstra DP, Monserud RA (eds) Forest growth and timber quality: crown models and simulation methods for sustainable forest management. Proceedings of the international conference Portland, August, 07th–10th 2007, USDA Forest Service Pacific Northwest Research Station: Gen. Tech. Rep. PNW-GTR-791, pp 23–33

Högberg K-A, Persson B, Hallingbäck HR, Jansson G (2010) Relationships between early assessments of stem and branch properties and sawn timber traits in a *Pinus sylvestris* progeny trial. Scand J for Res 25(5):421–431

Houllier F, Leban J-M, Colin F (1995) Linking growth modelling to timber quality assessment for Norway spruce. For Ecol Manage 74(1–3):91–102

Ikonen V-P, Kellomäki S, Peltola H (2009) Sawn timber properties of Scots pine as affected by initial stand density, thinning and pruning: a simulation based approach. Silva Fennica 43(3):411–431

Johansson E (2013) Computed tomography of sawlogs—knot detection and sawing optimization. Licentiate thesis, Department of Engineering Sciences and Mathematics, Luleå University of Technology, Skellefteå, Sweden

Johansson E, Johansson D, Skog J, Fredriksson M (2013) Automated knot detection for high speed computed tomography on *Pinus sylvestris* L. and *Picea abies* (L.) Karst. using ellipse fitting in concentric surfaces. Comput Electron Agric 96:238–245

Kenk G, Hradetzky J (1984, Behandlung und Wachstum der Douglasien in Baden-Württemberg. [Management and growth of Douglas-fir in Baden-Württemberg.] Mitteilungen der Forstlichen Versuchs- und Forschungsanstalt Baden-Württemberg, Abteilung Waldwachstum, Forstl. Versuchs- u. Forschungsanst. Baden-Württemberg, Freiburg i. Breisgau

Kenk G, Thren M (1984) Ergebnisse verschiedener Douglasienprovenienzversuche in Baden-Württemberg. Teil I. Der Internationale Douglasien-Provenienzversuch 1958. [Results of different Douglas-fir provenances tests in Baden-Württemberg. Part I: The International Douglas-fir provenance test 1958.], *Allgemeine Forst- und Jagdzeitung*, No. 7/8, pp 165–184

Kershaw JA, Maguire DA, Hann DW (1990) Longevity and duration of radial growth in Douglas-fir branches. Can J for Res 20(11):1690–1695

Kohnle U, Hein S, Sorensen FC, Weiskittel AR (2012) Effects of seed source origin on bark thickness of Douglas-fir (*Pseudotsuga menziesii*) growing in southwestern Germany. Can J For Res 42(2):382–399

Krähenbühl A, Kerautret B, Debled-Rennesson I, Mothe F, Longuetaud F (2014) Knot segmentation in 3D CT images of wet wood. Pattern Recogn 47(12):3852–3869

Krajnc L, Farrelly N, Harte AM (2019) The effect of thinning on mechanical properties of Douglas fir, Norway spruce, and Sitka spruce. Ann For Sci 76(1):1–12

Lin LIK (1989) A concordance correlation coefficient to evaluate reproducibility. Biometrics 45(1):255–268

Lin LI-K (2000) Correction. A note on the concordance correlation coefficient. Biometrics 56(1):324–325

Longo BL, Brüchert F, Becker G, Sauter UH (2019a) Validation of a CT knot detection algorithm on fresh Douglas-fir (*Pseudotsuga menziesii* (Mirb.) Franco) logs. Ann For Sci 76(2):28

Longo BL, Brüchert F, Stelzer A-S, Becker G, Sauter UH (2019b) Using computed tomography density profiles to identify whorls in douglas-fir trees: a graphical based approach. In: Wang X, Sauter UH, Ross RJ (eds) 21st International Nondestructive Testing and Evaluation of Wood Symposium.: General Technical Report FPL-GTR-272. Freiburg im Breisgau, Germany., U.S. Department of Agriculture, Forest Service, Forest Products Laboratory, Madison, WI, pp 535–541

Longuetaud F, Saint-André L, Leban J-M (2005) Automatic detection of annual growth units on *Picea abies* logs using optical and X-ray techniques. J Nondestr Eval 24(1):29–43

Longuetaud F, Mothe F, Leban J-M (2007) Automatic detection of the heartwood/sapwood boundary within Norway spruce (Picea abies (L.) Karst.) logs by means of CT images. Comput Electron Agric 58(2):100–111

Longuetaud F, Mothe F, Kerautret B, Krähenbühl A, Hory L, Leban JM, Debled-Rennesson I (2012) Automatic knot detection and measurements from X-ray CT images of wood. A review and valida-tion of an improved algorithm on softwood samples. Comput Electron Agric 85:77–89

Mäkelä A, Grace Deckmyn G, Kantola A, Campioli M (2010) Simulating wood quality in forest manage-ment models. Forest Syst 19 (special issue), 48–68

Mäkinen H, Colin F (1998) Predicting branch angle and branch diameter of Scots pine from usual tree measurements and stand structural information. Can J for Res 28(11):1686–1696

Nordmark U (2005) Value recovery and production control in the forestry-wood chain using simulation technique. Doctoral thesis/Luleå University of Technology

Nyrud AQ, Roos A, Rødbotten M (2008) Product attributes affecting consumer preference for residential deck materials. Can J for Res 38(6):1385–1396

Oja J, Skog J, Edlund J, Björklund L (2010) Deciding log grade for payment based on X-ray scanning of logs. Paper presented at the future of quality control for wood and wood products. The Final Confer-ence of COST Action E53. 4–7th May, Edinburgh

Pyörälä J, Kankare V, Vastaranta M, Rikala J, Holopainen M, Sipi M, Hyyppä J, Uusitalo J (2018) Com-parison of terrestrial laser scanning and X-ray scanning in measuring Scots pine (*Pinus sylvestris* L.) branch structure. Scand J For Res 33(3):291–298

R Core Team (2016) R: a language and environment for statistical computing. R Foundation for Statisti-cal Computing, Vienna, Austria

Rais A, Poschenrieder W, Pretzsch H, van de Kuilen J, Willem G (2014) Influence of initial plant den-sity on sawn timber properties for Douglas-fir (*Pseudotsuga menziesii* (Mirb.) Franco). Ann for Sci 71:617–626

Robinson D, Hayes A (2019) Broom: Convert Statistical Analysis Objects into Tidy Tibbles. R package version 0.5.2. https://CRAN.R-project.org/package=broom Accessed 15 September 2020

Roussel JR, Mothe F, Krähenbühl A, Kerautret B, Debled-Rennesson I, Longuetaud F (2014) Automatic knot segmentation in CT images of wet softwood logs using a tangential approach. Comput Electron Agric 104:46–56

Schad KC, Schmoldt DL, Ross RJ (1996) Nondestructive methods for detecting defects in softwood logs, Research Paper FPL-RP-546, Madison, WI. Forest Products Laboratory

Šeho M, Kohnle U (2014) Der Internationale Douglasien-Provenienzversuch 1958. Unterschiede in der Ausprägung von Ast- und Stammmerkmalen auf den südwestdeutschen Versuchsflächen" [The International Douglas-fir Provenance Trial 1958: Differences in the expression of branch and stem characteristics on the Southwest German trial plots], Allgemeine Forst- und Jagdzeitung 185(½), 27–42

Šeho M, Brüchert F, Kohnle U (2013) Computer tomography imagery. A tool for estimating characteris-tics of tree growth and timber structure? Forstarchiv 84(6):171–180

Shigo AL (1985) How tree branches are attached to trunks. Can J Bot 63(8):1391–1401

Stevenson M, Nunes T, Heuer C, Marshall J, Sanchez J, Thornton R, Reicziegel J, Robinson-Cox J, Sebastiani P, Solymos P, Yoshida K, Jones G, Pirikahu S, Firestone S, Kyle R, Popp J, Jay M (2018) epiR: Tools for the Analysis of Epidemiological Data. R package version 0.9–96. https://CRAN.R-project.org/package=epiR

Ursella E, Giudiceandrea F, Boschetti M (2018) A fast and continuous CT scanner for the optimization of logs in a sawmill. In: 8th conference on industrial computed tomography, Wells, Austria

Väisänen H, Kellomäki S, Oker-Blom P, Valtonen E (1989) Structural development of *Pinus sylvestrís* stands with varying initial density: a preliminary model for quality of sawn timber as affected by silvicultural measures. Scand J for Res 4(1–4):223–238

Wei Q, Chui YH, Leblon B, Zhang SY (2009) Identification of selected internal wood characteristics in computed tomography images of black spruce. A comparison study. J Wood Sci 55(3):175–180

Weiskittel AR, Maguire DA, Monserud RA, Rose R, Turnblom E (2006) Intensive management influence on Douglas fir stem form, branch characteristics, and simulated product recovery. NZ J Forest Sci 36:293–312

Wickham H (2016) ggplot2: Elegant graphics for data analysis, Use R! Springer, Cham

Wickham H, François R, Henry L, Müller K (2019) A grammar of data manipulation [R package dplyr version 0.8.1]

Yue C, Klädtke J, Kohnle U (2013) W+: Ein Kombinationsbasierter Wachstumssimulator für Fichten-, Douglasien- und Buchen-Bestände. [W+: A combination-based growth simulator for spruce, Douglas-fir and beech stands]. Allgemeine Forst- und Jagdzeitung 184(5):112–124

Publisher's Note Springer Nature remains neutral with regard to jurisdictional claims in published maps and institutional affiliations.